Atmos. Chem. Phys. Discuss., 11, 10557–10613, 2011
www.atmos-chem-phys-discuss.net/11/10557/2011/
doi:10.5194/acpd-11-10557-2011

Atmospheric Chemistry and Physics Discussions

Initiation of coalescence in a cumulus cloud: a beneficial influence of entrainment and mixing

W. A. Cooper[1], S. G. Lasher-Trapp[2], and A. M. Blyth[3]

[1]National Center for Atmospheric Research, Boulder CO, USA
[2]Purdue University, West Lafayette IN, USA
[3]National Centre for Atmospheric Science, University of Leeds, Leeds, UK

Received: 14 January 2011 – Accepted: 15 February 2011 – Published: 5 April 2011

Correspondence to: W. A. Cooper (cooperw@ucar.edu)

Published by Copernicus Publications on behalf of the European Geosciences Union.

Abstract

Although rain has been observed to form in warm cumulus clouds within about twenty minutes, calculations that represent condensation and coalescence accurately in such clouds have had difficulty producing rainfall in such a short time except via processes involving giant cloud condensation nuclei (with diameters larger than 2 µm). This model-based study explores a different possible mechanism for accelerating the production of warm rain, one that depends on the variability in droplet trajectories arriving at a given location and time in a cumulus cloud. In the presence of entrainment such droplets experience different growth histories, and the result is broadening of the droplet size distribution. That broadening favours coalescence, leading to embryos that grow to raindrops. These calculations do lead to production of rain that is within the lower range of observations for clouds of Florida, USA, the location on which the input conditions were based. The process emphasized in this study, the formation of drizzle via collisions among droplets in the main peak of the droplet size distribution, complements the growth of precipitation on giant nuclei, which is also an important source of the first rain in the case studied. The results indicate that the mechanism developed here should be considered an important influence on the formation of rain in warm clouds.

1 Introduction

Significant rain forms in warm cumulus turrets in less than 20 min, as documented by Laird et al. (2000); Blyth et al. (2003); Goke et al. (2007), and others. For example, Goke et al. (2007) used radar observations of single cells from the Small Cumulus Microphysics Study (SCMS) to show that the maritime clouds of that experiment increased in radar reflectivity from −5 dBZ to +7.5 dBZ in a characteristic time of 333 s. Calculations of the collision-coalescence process, such as those discussed in the review by Beard and Ochs (1993) and many others, required longer times unless the

ACPD
11, 10557–10613, 2011

early growth occurred on sufficient numbers of “giant nuclei,” particles larger than 2 µm in diameter (e.g., Ochs, 1978; Johnson, 1982; Lasher-Trapp et al., 2001).

Studies addressing this discrepancy in time have emphasized two additional candidates: (i) enhanced growth of a few of the largest cloud droplets caused by variability that results from either entrainment and mixing (Baker et al., 1980; Telford and Chai, 1980; Cooper, 1989, and others) or random droplet locations (Srivastava, 1989); and (ii) increase in coalescence rates that arise from turbulent enhancement of the collision rates or efficiencies (e.g., Saffman and Turner, 1956; Shaw et al., 1998; Pinsky et al., 1999b; Pinsky et al., 1999a; Wang et al., 2008). There are many other candidate mechanisms, such as electrical effects that can change the collision efficiencies or broadening arising from CCN components that inhibit growth. Despite these suggestions, the underlying discrepancy in time between observations and models has been a persistent concern for decades.

In the study presented in this paper, only the effect of variability associated with entrainment will be considered. Other contributions can be explored once the importance of that process is established, but such explorations will be deferred to future work. Because entrainment reduces the liquid water content of the cloud, it is clearly detrimental to precipitation formation (cf., e.g., Jonas and Mason, 1982, 1983) and must be included in a realistic study. However, given that entrainment occurs, other effects might broaden the droplet size distribution or introduce large droplets, aiding the development of precipitation (Baker et al., 1980). The “central premise” of the present work, discussed in more detail in the next section, is that combining droplets that have grown along different trajectories through the entraining cloud will produce a broader size distribution more conducive to coalescence.

ACPD
11, 10557–10613, 2011

2 The central premise

The central premise investigated in the present study is that entrainment and associated mixing in clouds broaden the droplet size distribution in ways that introduce some relatively large drops into regions with high liquid water content, and the resulting growth of those larger droplets accelerates the formation of raindrops. The process that is key to this premise is turbulent diffusion of cloud droplets, which causes droplets that are within range of colliding with each other to have come together after experiencing different growth histories. In the terminology of Cooper (1989), entrainment causes droplets to experience different integral supersaturations over time while moving along nearby trajectories.

Turbulent diffusion of particles originating from a localized source is well known to lead to dispersion of smoke or other particles, in a manner similar to that illustrated in Fig. 1a. The calculations leading to the trajectories in this figure were based on these conditions: mean updraft of $3\,\mathrm{m\,s^{-1}}$; standard deviation (in all three components of the wind) of $0.36\,\mathrm{m\,s^{-1}}$; and a Lagrangian correlation time of 37 s. These values were chosen to correspond to a value of subgrid-scale turbulent kinetic energy E of $0.2\,\mathrm{m^2\,s^{-2}}$ at scales below $\Delta = 25\,\mathrm{m}$ (the grid size in the cloud simulation that follows) and to an eddy dissipation rate of $(2E/3)^{3/2}(2\pi/\Delta) = 1.22 \times 10^{-2}\,\mathrm{m^2\,s^{-3}}$, in a range measured in many cumulus clouds (e.g., MacPherson and Isaac, 1977). The calculations were performed by taking into account the correlation time, as described by Lasher-Trapp et al. (2005). If droplets follow the air trajectories (as is the case in the early stages of droplet growth), this calculation serves to illustrate that cloud droplets originating just above cloud base at a given location will diffuse over significant distances as they move through the cloud, spanning in this case more than 100 m after an ascent of 6 km and a time of 30 min.

Figure 1b combines the plumes generated at seven different locations at cloud base at 10-m intervals. The droplets that would be observed at a central location (e.g., abscissa and ordinate of 0 m and 3000 m, respectively) would originate at different

Discussion Paper | Discussion Paper | Discussion Paper | Discussion Paper |

ACPD

11, 10557–10613, 2011

Initiation of coalescence in a cumulus cloud

W. A. Cooper et al.

cloud-base locations, yet would be observed together if the droplet size distribution were measured in a small sample volume centred at that location. This point is illustrated also by Fig. 1c, where only the trajectories that pass within 1 m of a specified reference point are shown. The trajectories can be calculated both forward and backward in time from that point because the equations are reversible in time if the characteristics of the turbulence remain the same as in this simple example. This figure serves to emphasize that the droplet size distribution present at a given point in a cloud consists of an ensemble of droplets that experience varying trajectories both before and after reaching that point.

Such a process does not in itself lead to substantial broadening, because it has been argued convincingly that, for adiabatic ascent, droplets experiencing faster ascent grow faster in a compensating way such that droplets reaching a given altitude have almost the same size (Bartlett and Jonas, 1972). However, entrainment can break the otherwise strong connection between ascent rate and growth if nearby droplets experience different growth histories. Trajectories in the ensemble reaching a reference point can encounter stronger or weaker evaporation associated with entrainment, and the supersaturation may be enhanced in subsequently ascending regions of clouds that have been influenced by entrainment. Variations in the updraft at cloud base can also contribute to variability in size by causing different fractions of the cloud condensation nuclei to be activated. In these ways, droplet size distributions can be broadened toward both smaller and larger sizes, as will be illustrated further by calculations reported in Sect. 5.

In the present study a combination of models is used to investigate this premise in quantitative terms, in an attempt to simulate conditions in a warm cloud that was observed to produce rain. The aim is to determine if rain can be produced by the proposed mechanism in a realistic time.

ACPD
11, 10557–10613, 2011

3 The approach and model framework

Modelling of the initiation of coalescence requires accurate calculation of the condensation process, which can be compromised unless the size of the bins used for droplet size is very small. The cloud motions that bring about entrainment and associated dilution of the cloud, prominent in all small cumulus cells, must also be modelled for a reliable comparison.

To represent the collision-coalescence process adequately, another long-standing problem must also be addressed: What are the factors controlling the development of the droplet size distributions in the absence of coalescence? This was the problem addressed in two earlier papers, Cooper (1989) and Lasher-Trapp et al. (2005). On the basis of turbulent diffusion as illustrated in the previous section, it was argued that the droplet size distribution at a particular location in a cloud arises from the collocation of an ensemble of droplets that have experienced variability in their growth conditions before coming together at that point. Those papers suggested that variability in the trajectories of cloud droplets reaching a given location in a cloud contributes to and perhaps accounts for the observed broadening of droplet size distributions.

Lasher-Trapp et al. (2005), hereafter LCB05, used the same two-component modelling framework to be used here, a 3-D dynamical cloud model coupled with a Lagrangian microphysical model, to develop quantitative predictions of droplet size distributions resulting from entrainment and mixing in small cumulus clouds. The cloud model represented turbulent cloud dynamics with entrainment but parametrized microphysical processes such as condensation, while the microphysical model performed explicit microphysical calculations (including the activation of cloud condensation nuclei (CCN), condensation or evaporation, and effects of entrainment and mixing) along trajectories constrained to match the thermodynamic and kinematic fields of the cloud model. The resulting droplet size distributions replicated key features of classic observations of cloud droplet size distributions in small cumuli such as those of Warner (1969), including broad distributions, the continued presence of small droplets high in the clouds, and the bimodal structure. These features in the modelled distributions originated from the variability in the supersaturation histories experienced by the droplets, variability that was introduced by entrainment and mixing as the droplets moved through the cloud, and from the activation of entrained CCN.

In the present study, sedimentation of drops is now incorporated in an approximate way into the model framework, enabling the calculations to be carried forward to the point of formation of the first raindrops. The Lagrangian microphysical model represents both diffusional and coalescence growth of droplets to raindrop embryos (here taken to be drops larger than 40 µm in diameter). To determine if the embryos produced in the microphysical model can lead to significant rain, they are inserted into the cloud-water fields of the 3-D cloud model where they grow by continuous collection as in the calculations of Lasher-Trapp et al. (2001).

The cloud model used to represent kinematic and thermodynamic properties of the cloud is the Straka Atmospheric Model (Straka and Anderson, 1993) as modified by Carpenter et al. (1998), with increased resolution (25 m) to improve the representation of small-scale features. This form of the model uses bulk microphysics to represent cloud condensation processes without autoconversion, because the earliest raindrops are produced explicitly within the microphysical model and later grow by continuous collection in the cloud-water fields of the cloud model. The cloud model provides a realistic representation of entrainment and provides an estimate of the subgrid-scale turbulence for use in calculations of trajectories and microphysical evolution.

The 10 August 1995, 1408 UTC thermodynamic sounding from the Small Cumulus Microphysics Study (Florida, USA, 1995) was used for the case to be presented. This cloud was chosen because radar observations showed rapid development of rain and because modeling readily produced high liquid water contents (>3 g m^{-3}). Study of another cloud with lower liquid water content and lifetime that did not develop precipitation was presented at the Fifteenth International Conference on Cloud Physics in 2008; that study led to selection of this more persistent cloud for the present study. As in LCB05, Gaussian heat and moisture fluxes are inserted at the bottom of the cloud model domain (located at 4 m MSL) to produce the cloud.

ACPD
11, 10557–10613, 2011

On this day, a particular multi-thermal cloud developed that was about 2 km wide, with cloud base at 730 m MSL, maximum cloud top at 4500 m, and peak radar reflectivity of 40 dBZ. The cloud dissipated about 20 min after its first appearance on radar. The modelled cloud was tuned (via adjustment of the forcing) to have very similar characteristics: multiple thermals up to 2 km wide, cloud base altitude 725 m, cloud top 4600 m, and about 20 min lifetime before abrupt dissipation (Fig. 2). It exhibits significant variability in the spatial distribution of cloud water as a result of entrainment, as shown in Fig. 3.

To represent the growth of cloud droplets with the desired accuracy, the Lagrangian or parcel [1] model discussed by Cooper et al. (1997) and LCB05 was used to represent droplet growth along trajectories in the cloud model. This division into two models was necessary because only the highest-resolution calculations can provide realistic representation of the droplet-growth process. By using bins moving in size in the microphysical model, where each bin corresponds to a specific activation time step at cloud base, it is possible to represent growth by condensation without reassigning droplets to bins.

Appendix A documents some changes made to the Lagrangian microphysical model since its description in LCB05 and Cooper et al. (1997). The most significant are these:

– Reactivation of evaporated droplets (e.g., during inhomogeneous evaporation) was incorporated in a straightforward way by using a separate size-distribution array, like that for cloud-base CCN, to represent both the entrained CCN and those produced by evaporation of droplets. (LCB05 included only initial activation of entrained CCN.) This second array was used to create new droplets when the

[1] This is a parcel model in the sense that a population of droplets formed at cloud base is tracked through the cloud without mixing with the environment except for inclusion of dilution and evaporation as required by entrainment. In reality, mixing of droplets will occur all along such trajectories, usually adding to the variability. The approach taken is a first approximation to the effects of variability in trajectories, but an exact simulation would have to represent mixing of droplets at all times along the trajectories.

ACPD
11, 10557–10613, 2011

supersaturation required such activation.

- Several changes were made to the treatment of inhomogeneous evaporation, as described in detail in Appendix A1. The basic requirement for inhomogeneous evaporation, from Baker and Latham (1979), is that the time scale for evaporation of droplets be short compared to the time scale characteristic of the turbulence responsible for the mixing, causing some droplets to evaporate completely while others are unaffected. However, the evaporation times vary with size, so calculations that represent inhomogeneous evaporation should be applied only to those droplets small enough to evaporate on the time scale of the turbulence. It is particularly important to exclude droplets growing on giant CCN if they are too large to evaporate on this time scale, because otherwise the effect of giant nuclei will be under-represented.

- The assumed shape of the giant-nucleus portion of the CCN size distribution was changed, as described in Appendix A3, to reflect better the conditions expected in the study location.

To estimate the amount of rain produced in the cloud, the drops large enough to have significant collection efficiency (i.e., those with diameters greater than 40 µm) are inserted into the cloud-model fields and allowed to grow along trajectories in the manner discussed by Lasher-Trapp et al. (2001). This last step is used only to evaluate if the rainfall produced can be considered realistic for a cloud of this type, as discussed in Sect. 6.

4 Typical trajectories and trajectory following

The trajectories followed by the Lagrangian microphysical model were generated as described in LCB05 and in a manner similar to that used to generate Fig. 1. They were calculated backward in time from a 9×12 horizontal grid of reference points placed 100 m apart. The grid was placed to cover the cloud at 3000 m MSL. To each reference

ACPD
11, 10557–10613, 2011

point, (typically) 500 trajectories [2] were generated, each leading to the reference point exactly 10 min after the first appearance of the cloud. Of these, 57 reference points were inside the simulated cloud, which at 10 min had just moved through this altitude, and those points form the basis for the calculations that follow. Four of these points are shown in Fig. 4, where some of the variability of the trajectory paths and the influence of entrainment are evident. Loops in the trajectories can arise from the thermal circulation, eddies, or mixing between updrafts and downdrafts. Regions of lower cloud water along the trajectories result from entrainment and mixing.

For further illustration, trajectories are picked that originate at cloud base (928 hPa, 22.4 °C and 0.7 km MSL) and rise to 705 hPa, 10 °C, and about 3 km MSL. Figure 5a and 5b show some trajectories that arrive at a reference point about 0.6 km from the centre of the cloud. Figure 5a illustrates that the trajectories vary significantly in the times when they moved through cloud base: Some droplets arriving at the reference point moved through cloud base only 300 s earlier, while others rose for more than 500 s. Figure 5b shows that the wet-equivalent potential temperature (Θ_q) history of these droplets also varied significantly: Most experienced a rapid decrease from 200–100 s before arriving at the reference point, as a result of a significant entrainment event, after undergoing relatively little change before then, but there are some large departures from that mean behaviour including some that decrease and subsequently increase in Θ_q. (See Appendix A2 for discussion of how such points are handled.) These two plots illustrate that there is substantial variability in the time histories of droplets reaching the reference points, both in available growth time and in thermodynamic properties of the environment.

[2] Although the goal was to have 500 trajectories reaching a given reference point, in some cases it was only possible to generate half of this number, or even less, especially when the point was near a region of very small liquid water content where most of the air trajectories originated outside the cloud (with the entrained air), rather than in cloudy air that had ascended from the cloud base. Tests showed that the variability was captured well using only 100 trajectories per reference point.

ACPD
11, 10557–10613, 2011

5 Cloud droplet size distributions

5.1 Adiabatic ascent

For reference, and to illustrate the ability of the Lagrangian microphysical model to simulate very narrow size distributions, the development of the droplet size distribution during adiabatic ascent of a parcel is shown first. For most calculations presented in this paper, the Lagrangian model was run by imposing the conditions of a trajectory through the cloud-model fields, but in this test case the parcel rose as determined by buoyant ascent without entrainment. Such ascent required 254 s in an average updraft of about 9 m s^{-1} to reach the same reference point discussed previously (at 3 km MSL or about 2.3 km above cloud base). The CCN cumulative supersaturation distribution, estimated from measurements made by Yum and Hudson, was taken to be $N(\mathrm{SS}) = N_0(\mathrm{SS}/1\%)^k$ with respective values of 365 cm^{-3} and 0.23 for N_o and k. (See also Appendix A3.) This was one of the lowest CCN concentrations observed during the SCMS (Yum and Hudson, 2001) and is consistent with the maritime conditions of their summary.

Figure 6 shows the result of this calculation. The resulting size distribution is exceptionally narrow: The standard deviation in droplet diameter is only about 1% of the mean diameter. The plot also shows the appearance of features in the droplet size distribution at diameters nearly at but slightly below the sizes of 39, 45, and 50 µm that would be expected to arise from coalescence of 2, 3, and 4 of the droplets from the main peak. These are the products of the coalescence process in this adiabatically ascending parcel (as verified by suppressing coalescence in another calculation), but the concentrations of droplets larger than those in the central peak is very low. The concentration of droplets larger than 40 µm in diameter was 0.016 cm^{-3}; for those exceeding 50 µm the concentration was only 0.0006 cm^{-3}. (These sizes will be used as references for comparison to other cases to be presented.) Thus, despite the high liquid water content (4.3 g m^{-3} at the end of this ascent), negligible production of drizzle

ACPD
11, 10557–10613, 2011

or initiation of coalescence occurred in the calculation in the time required for ascent from cloud base.

This is a good illustration of the well known problems that inhibit coalescence in calculations such as these. For diameters below 30 µm, collection efficiencies are low (less than 10%), and both collection efficiencies and fall-speed differences minimize for droplet pairs that are nearly the same size, so growth rates by coalescence are slow even when the liquid water content is high.

5.2 Representation of evaporation caused by entrainment

As discussed by LCB05, the nature of the evaporation that occurs with entrainment affects the resulting size distribution, particularly in regard to the degree that the mixing leads to "inhomogeneous" evaporation as characterized by Baker and Latham (1979). Full exploration of this influence will not be attempted in this paper, but there is recent guidance in a paper by Andrejczuk et al. (2006) that suggests the specific approach taken in the following. Their results suggest that mixing proceeds in a nearly universal way for a wide range of mixing proportions, and that for low intensity turbulence (i.e., turbulent kinetic energy less than about $1.6 \times 10^{-4}\ \mathrm{m^2\,s^{-2}}$) the results are approximately midway between the extreme inhomogeneous and fully homogeneous results, with the ratio of the mean droplet concentration to the initial droplet concentration decreasing approximately in proportion to the liquid water content. At higher turbulent kinetic energy, the results are initially characterized by homogeneous evaporation, as expected by the dimensional arguments underlying the inhomogeneous-evaporation process, after which there is a transition to a similar linear behaviour.

In the Lagrangian microphysical model, it is possible to replicate this behaviour by representing the mixing process in the following way:

ACPD
11, 10557–10613, 2011

1. As described in Sect. 3 and more fully in Appendix A1, homogeneous evaporation is forced (at each time step) for droplets with evaporation time constants longer than the integral time scale for the turbulence.

2. For droplets smaller than the threshold defined in the preceding step, the mixing is assumed to lead to 50% homogeneous and 50% inhomogeneous evaporation. Specifically, the calculation determines the fraction of droplets that would evaporate completely to saturate the mixture (as for the extreme inhomogeneous case), but then evaporates only 50% of that fraction of droplets.

3. The resulting temperature and vapour pressure are then carried forward so as to drive homogeneous evaporation of the remaining droplets.

When the resulting concentration (excluding newly activated droplets produced on entrained CCN) and liquid water content are plotted in the manner of Andrejczuk et al. (2006), the results are quite similar to their universal plots (their Figs. 6–8). This and other results that suggest a combination of homogeneous and inhomogeneous evaporation (e.g., Jensen et al., 1985; Lehmann et al., 2009) argue for the realism of this representation of the mixing process. Other choices, investigated but not presented here, do not change the conclusions of this paper.

5.3 Single trajectories with entrainment

The case of adiabatic ascent can be compared to a more realistic trajectory from the cloud simulation, which is shown in Fig. 7. A droplet following this trajectory ascends for about 362 s vs. 254 s in the adiabatic-ascent case. It also experiences entrainment events that reduce Θ_q, notably at about −100 s. This trajectory led to a final liquid water content of 3.54 g m^{-3}, about 82% of the adiabatic value. The resulting size distribution, shown in Fig. 8, has almost the same mean diameter as that for adiabatic ascent, but the distribution is now significantly broader (with a standard deviation about 18% of the mean diameter vs. 1% for the adiabatic case). The majority of this

ACPD
11, 10557–10613, 2011

broadening occurs as a result of activation of CCN that are entrained along the trajectory; these contribute about 20% of the final droplet concentration and account for the droplets smaller than the mode in Fig. 8. However, significantly, the number of drops with diameter greater than 40 µm is now also larger, about five times the result for adiabatic ascent. The droplet number concentration along this trajectory is less than the adiabatic case (218 vs. 272 cm^{-3}), primarily as a result of dilution from entrainment and mixing. The longer ascent time (362 s vs. 254 s for the adiabatic case) along a more meandering trajectory (also a result of entrainment and mixing) produces more collision-coalescence events before the cloud reaches a given altitude. The production of drizzle remains small, however, because there is not enough breadth in the droplet sizes to support significant growth by collision-coalescence.

Figure 9 shows the droplet size distribution that resulted from an entrainment sequence that reduced the droplet concentration to about two-thirds of that for the adiabatic trajectory. In this case, a lower concentration of entrained CCN is activated, which favours growth of droplets already present to larger sizes. Although the water content is slightly lower than the preceding case, there is more growth to sizes larger than the primary peak, so there are more embryos for continued growth.

The conclusion from these two examples is that entrainment not only reduces the liquid water content, but also, in some cases, leads to production of larger droplets at a given altitude. The subsequent growth of those droplets will be faster in the case with higher liquid water content, so this favoured production of embryos in some regions of low liquid water content competes with the subsequent speed at which those embryos can continue to grow.

5.4 Ensembles of trajectories

Figures 8 and 9 result from following individual trajectories, but the ensemble contributing at any point must be considered instead to determine if there is any acceleration of coalescence. To that end, calculations similar to those shown in the preceding figures were carried forward from the point of origin of each of the trajectories leading to each

ACPD
11, 10557–10613, 2011

of the reference points (cf. Sect. 4). The results at each reference point were then averaged to obtain an estimate of the droplet size distribution present at those points, as in LCB05; this is equivalent, in an averaged sense, to randomly selecting droplets from the ensemble to include.

An example is shown in Fig. 10. The mean droplet size distribution included significant large-size and small-size portions of the size distribution in addition to the main peak. The distribution is substantially broader than any of the individual distributions (e.g., Figs. 8 and 9), both in terms of the full distribution and in terms of the breadth of the central peak. This size distribution has multiple peaks and substantial breadth towards both smaller and larger droplet sizes and so appears realistic in comparison to size distributions often measured.

From each of these reference points, a single trajectory determined from the mean motion in the cloud model was then followed forward for two more minutes in the Lagrangian model with explicit microphysics, to produce a size distribution like that shown in Fig. 11. The reason for this extension was to allow an opportunity for coalescence to occur in the broadened size distribution. The end point of this 2-min extension will be called the "insertion point" because from there the embryos will be inserted back into the cloud-model fields for continued growth. This is a compromise forced by the need to perform microphysical calculations with uncompromised accuracy, which in the framework used does not allow consideration of sedimentation and so must be abandoned once droplets grow to sizes where sedimentation is significant.

A comparison of Figs. 10 and 11 shows that the size distribution produced by the various trajectories at a reference point broadens still more as it is carried forward to the insertion point, now just as a result of coalescence. In Fig. 11 the concentration of droplets with diameters above 40 µm is 0.916 cm^{-3}, vs. 0.146 cm^{-3} before the additional two minutes of growth.

Discussion Paper | Discussion Paper | Discussion Paper | Discussion Paper |

ACPD

11, 10557–10613, 2011

Initiation of coalescence in a cumulus cloud

W. A. Cooper et al.

5.5 Summary of key points

The key points from this section are these:

– Little coalescence growth occurs in the simulated parcel ascending adiabatically, and the small number of larger droplets that appear are located in peaks that are mass-multiples of the central peak.

– Entrainment alone can accelerate the production of larger droplets, even while reducing the liquid water content, by producing longer trajectory paths and thus more time for collision-coalescence as the droplets ascend through the cloud. The production of larger drops for initiating collision-coalescence is also sometimes enhanced by evaporation associated with entrainment, especially when that evaporation has a partly inhomogeneous character.

– Combining trajectories as in LCB05 leads to significant and realistic broadening, as argued previously, and also to the appearance of droplets with sizes significantly larger than the modal size. The variability introduced along turbulent and diffusing trajectories not only introduces substantial broadening into droplet size distributions but also accelerates the formation of droplets with appropriate sizes to act as coalescence embryos for growth to rain.

6 Results carried forward to rainfall in the cloud

6.1 Basis for the calculations

In order to determine if the embryos formed as in the preceding section can lead to significant rainfall, the calculations that follow evaluated the growth of those embryos by inserting them into the cloud-water fields of the cloud model. Lasher-Trapp et al. (2001) described the approach, which is continuous collection with consideration of collection efficiencies for the parametrized size distributions of the model cloud droplets. Up

Discussion Paper | Discussion Paper | Discussion Paper | Discussion Paper |

ACPD

11, 10557–10613, 2011

Initiation of coalescence in a cumulus cloud

W. A. Cooper et al.

to the insertion points, fall speeds of the droplets were neglected when determining trajectories because the fall speed of a droplet 40 µm in diameter is only about 5 cm s^{-1} (Beard (1976), negligible compared to the cloud simulation velocities. However, for embryos growing to raindrops, fall speeds become comparable in magnitude to air motions in the cloud, so the calculated drop trajectories through the cloud must then take into account the size and fall speed of individual drops as well as the air motions in the cloud. The approach taken here is less suited to study of the growth on giant nuclei because some giant nuclei grow to sizes where sedimentation is important before the insertion points. However, the emphasis here is on the high concentration of small embryos that form primarily by coalescence among droplets in the main peak of the size distribution, and for those this approach is appropriate.

The calculated growth extends until the liquid water content of the model cloud became depleted at the end of the cloud lifetime (cf. Fig. 2f), about 10 min after the insertion time. Because the total precipitation mass remained a small part of the cloud water, no feedback was needed to represent either depletion of the cloud water by this growth or possible dynamical effects on the cloud model. The size distributions that resulted at the end of these calculations then form the basis for the estimates of rainfall, rainrate and precipitation efficiency developed in this section.

6.2 Resulting drop size distributions

Figure 12 shows the average size distribution of the embryos at the 57 insertion points and the final sizes after nearly 10 min of additional growth by continuous collection of cloud water. The average cumulative size distribution of all the initial embryos at the insertion points shows that over 0.5 cm^{-3} drops with diameters of 40 µm and larger were inserted into the continuous collection model, and nearly 6 cm^{-3} of these exceeded 500 µm in diameter at the end of the calculations. The amount of water mass contained in the precipitation embryos, initially only 0.003 g m^{-3}, grew to 0.5 g m^{-3} after ten additional minutes of growth (where the units refer to the mass that would be

ACPD
11, 10557–10613, 2011

Initiation of coalescence in a cumulus cloud

W. A. Cooper et al.

present if the raindrops, now distributed through the cloud as a result of their different fall speeds, were returned to the original volume of air at the insertion point). The instantaneous rainrate, calculated by averaging the results at the 57 insertion points, was $2\,\mathrm{mm\,h^{-1}}$. Tests with two other reference grids produced higher rain rate values, with a maximum of about $6\,\mathrm{mm\,h^{-1}}$.

To check that the minimum size used for embryos was adequate, the calculations were repeated with embryo sizes of 30, 40, and 60 µm diameter. The result was that the contribution from droplets smaller than 40 µm diameter was negligible, so this choice includes essentially all the rain production. Figure 13 shows one example of how little such embryos grew, as compared to those at 50 µm diameter and larger. At the time when the continuous collection calculations were halted, the largest embryos had fallen beneath the cloud base, those in the middle of the range had fallen through most of the cloud, but the smallest embryos were still in the upper parts of the cloud, not far from where they were released. The small fall speeds and collection efficiencies of such drops prevent their growth in a continuous-collection calculation such as this, although a weakness of the calculation and a likely reason that it underestimates the rainfall is that it does not permit collisions among the embryos that might stochastically produce larger drops with larger fall speeds and collection efficiencies.

A consistent result among numerous runs with the modelling framework, including results from a cloud simulation different from that shown here and results with different times and locations for insertion points in the simulated cloud, is that the number of embryos produced by the variability in supersaturation histories resulting from entrainment and mixing in a region of the cloud is not a good predictor of the amount of precipitation that eventually will result from such embryos. Although there were more than $0.5\,\mathrm{cm^{-3}}$ embryos at numerous insertion points (Fig. 14a), most grew little by collection of cloud water as they fell through the cloud. The highest concentrations of such embryos often followed strong entrainment events, but the embryos then tended to reside in regions of small liquid water content, at least initially (Fig. 14b), limiting further growth by collection of smaller cloud droplets. Small and Chuang (2008) reported similar findings

Discussion Paper | Discussion Paper | Discussion Paper | Discussion Paper |

ACPD

11, 10557–10613, 2011

Initiation of coalescence in a cumulus cloud

W. A. Cooper et al.

in trade-wind cumuli: The largest drops were present near the cloud top in regions of lower liquid water content.

Embryos from such regions nevertheless produced a significant part of the precipitation, because some of the embryos subsequently fell through regions of higher liquid water content. This is illustrated in Fig. 14. The circled points in Fig. 14a produced nearly equivalent precipitation masses although one point had an order of magnitude more embryos than the other. These same two points are circled in Fig. 14b, which shows that the point with the smaller number of embryos initially resided in a region of much more cloud water where the embryos could grow to larger sizes more quickly than the point with the greater number of embryos residing in a region of less cloud water.

The scatter in these plots also demonstrates another tendency in the results: A small number of preferred locations produced the majority of the initial precipitation. Three points were responsible for 61% of the total precipitation mass created among this set of 57 insertion points. These results suggest that the majority of the earliest raindrops are produced in a few rare regions within a cumulus cloud, as would be consistent with the difficulty in finding them with in situ cloud observations (e.g., Beard and Ochs, 1993; Small and Chuang, 2008, and references therein).

6.3 Estimated rainfall

For use in extrapolating the results over the lifetime of the cloud, the mass flux of precipitation M and rainrate R were calculated from all of the drops larger than 100 µm diameter, located anywhere in the cloud at the time the continuous collection model is halted, from

$$R = \frac{M}{\rho_\mathrm{w}} = \frac{1}{\rho_\mathrm{w}} \sum_i n_i m_i v_i \tag{1}$$

where n_i, m_i, and v_i are respectively the number concentration, mass, and fall speed of drops in each size class i and ρ_w is the density of water. This mass flux and rainrate, in

ACPD
11, 10557–10613, 2011

this particular case equivalent to $1644\,\mathrm{kg\,s^{-1}}$ and $2\,\mathrm{mm\,h^{-1}}$ respectively, then represent quantities resulting from the embryos inserted at the insertion time.

These drops, however, are replaced by others as the air motions bring new condensate to this level. If, for example, a $5\,\mathrm{m\,s^{-1}}$ updraft is present at a given 25-m grid box, the full grid box at that altitude is replaced every 5 s, so the resulting rainrate seen throughout the cloud receives an independent contribution from this grid box each 5 s. The total precipitation from this grid box is then related to the cumulative mass flux , if all the precipitating mass remains in the cloud.

If it is assumed that the condensate has negligible fall speed in comparison to the updraft speed w, the condensate flux through the reference level is $F = \chi w$ where χ is the liquid water content. A precipitation efficiency can then be determined by the ratio $\epsilon = M/F$. This is an unconventional definition of precipitation efficiency because the precipitating mass flux is calculated from the fall velocities rather than relative to a ground-referenced coordinate system. At the reference level and time, the condensate flux F obtained in this way is $7926\,\mathrm{kg\,s^{-1}}$, yielding a precipitation efficiency of 21%. Estimates of similar magnitude have been documented for deeper cumulonimbi based on observations (e.g., Fankhauser, 1988) and numerical modelling (e.g., Ferrier et al., 1996).

If all precipitation so formed eventually reaches the ground and all precipitation forms from drops passing through the reference level at 3000 m MSL, the total rainfall can be estimated from $T = \int \epsilon(t) F(t) dt$. Because about 30 000 trajectories were used to estimate the rainfall at a single time, repeating such calculations at regular intervals throughout the cloud lifetime was impractical. Instead, an approximate measure (T_e) was obtained by assuming that the precipitation efficiency remained constant: $T_e = \epsilon_0 \int F(t) dt$ where ϵ_0 is the precipitation efficiency calculated at the reference level and time. For this estimate, the time integral extends from when condensate first reached the reference level until the condensate flux decreased to 66% of its peak value at that level, a period of 7.5 min. Values of F were computed at the reference level from the simulated cloud in 30 s intervals. The lifetime rainfall was

ACPD
11, 10557–10613, 2011

Initiation of coalescence in a cumulus cloud

W. A. Cooper et al.

approximately 0.4 mm averaged over the insertion points (which covered a total area of about 0.6 km^2), leading to a total rain mass of about 2.4×10^5 kg. This rain mass is small and well below the rainfall that would be estimated from the radar reflectivity of the actual cloud on which this study was based. However, the significance of this result is that rainfall was initiated in less than 20 min, a result that has been difficult to achieve in realistic simulations of the development of warm rain.

6.4 Summary of key points

- Significant numbers of large drops (exceeding 0.1 cm^{-3}) capable of initiating coalescence can be produced in the upper regions of a cumulus cloud as a result of entrainment and mixing. Those drops larger than 40 µm diameter appear to have the most influence on rain initiation.

- A trade-off exists between the production of coalescence embryos by entrainment and mixing and the amount of cloud water they can collect to produce precipitation. In most cases, regions where substantial entrainment and mixing has produced many embryos also have little remaining cloud water in the smaller droplet sizes available to be collected.

- Rare events, where entrainment and mixing result in many coalescence embryos that are transported later into regions of high cloud water content, appear to be responsible for much of the precipitation. These events can account for significant rainfall rates over the short lifetime of a cumulus cloud.

- Although rainfall is initiated, the amount is lower than expected for such a cloud.

Discussion Paper | Discussion Paper | Discussion Paper | Discussion Paper |

ACPD
11, 10557–10613, 2011

Title Page
Abstract | Introduction
Conclusions | References
Tables | Figures
◀| |▶
◀ ▶
Back | Close
Full Screen / Esc
Printer-friendly Version
Interactive Discussion

7 Sensitivity to some factors that influence the formation of rain

7.1 Coalescence

The preceding argument is based on the formation of precipitation embryos by coalescence and the subsequent growth of those embryos to rain. To support that this is the correct interpretation of the results, the calculations leading to Fig. 11 were repeated with coalescence suppressed. Figure 15 shows the resulting drop size distribution for the set of trajectories reaching one reference point. With coalescence, the concentration of embryos that grew larger than 40 μm in diameter was 1.041 $\mathrm{cm^{-3}}$, and 0.030 $\mathrm{cm^{-3}}$ grew larger than 50 μm in diameter. With coalescence suppressed in the calculations, the corresponding concentrations were only 0.0025 and 0.00013 $\mathrm{cm^{-3}}$. When all reference points were averaged, the corresponding concentrations were 0.330 $\mathrm{cm^{-3}}$ and 0013.6 $\mathrm{cm^{-3}}$ with coalescence but only 0.046 and 0.0006 $\mathrm{cm^{-3}}$ without coalescence. With coalescence suppressed, the rainrate and total rainfall were only 0.01 $\mathrm{mm\,h^{-1}}$ and 0.003 mm, respectively, much less that the corresponding values of 1.9 $\mathrm{mm\,h^{-1}}$ and 0.4 mm obtained for the standard calculation. The estimated precipitation efficiency was only 0.1% without coalescence, vs. 21% for the standard calculation. These results support the interpretation that coalescence leads to most of the embryos involved in the production of rainfall in these calculations.

7.2 Giant nuclei

Both in observations of some small cumulus clouds (Caylor and Illingworth, 1987; Illingworth, 1988; Illingworth and Caylor, 1988; Knight et al., 2002) and in these calculations, giant nuclei play a significant role in the early development of precipitation, especially in the formation of the largest drops. The concentration used for such nuclei in this study is based on the estimates of Lasher-Trapp et al. (2002) which are lower than the estimates for generation from the sea surface under high-wind conditions (Johnson, 1982; Woodcock, 1952, 1953, 1978; Woodcock et al., 1971) but are appropriate

ACPD
11, 10557–10613, 2011

for low-to-moderate wind, as argued in Appendix A3. This comparison suffers from the poor representation of the growth of the larger droplets formed on giant nuclei, arising from the neglect of the fall speed of such drops prior to the insertion point, so this comparison is intended only to determine if such nuclei completely dominate the rain-formation process.

To determine the influence of the assumed concentration of giant nuclei in these results, those nuclei larger than 2.0 µm in diameter were eliminated from the assumed CCN distribution and the calculations leading to rain were repeated. Figure 16 shows the resulting cumulative drop size distribution averaged for all the size distributions at the insertion points. The giant nuclei account for the difference at largest sizes, but there is little difference for drop diameters less than about 70 µm and the total concentrations of embryos exceeding, respectively, 40 µm and 50 µm in diameter change only from 0.330 cm^{-3} and 0.0135 cm^{-3} to 0.317 cm^{-3} and 0.0113 cm^{-3} when giant nuclei were eliminated. However, the giant nuclei still have a strong influence on the initial formation of rain in these calculations. The rainrate and total rainfall produced in the calculation without giant nuclei were only 0.7 µm and 0.1 mm, while the calculated precipitation efficiency was only 8%. (The corresponding numbers with giant nuclei included were 1.9 mm h^{-1}, 0.4 mm, and 21%.) While the number of drizzle-size drops is dominated by coalescence growth from the main peak, the giant nuclei still account for a majority of the rainfall that develops in this model cloud. In subsequent development of precipitation in longer-lived clouds, the continued presence of drizzle will contribute to precipitation development, but the larger drops developing from the giant nuclei may also shatter into smaller drops either spontaneously or as the result of collisions, so it is difficult from these calculations to estimate the relative importance of the two sources of raindrop embryos over the life-cycle of such a cloud. There are also other effects not explored here that can increase the production of drizzle via collisions in the main peak of the droplet size distribution, especially the effects of turbulence on collision efficiencies and rates.

ACPD
11, 10557–10613, 2011

7.3 Broadening of the droplet size distribution by variability in trajectories

To assess the importance of the broadening of the droplet size distribution that occurs from variability in trajectories reaching a specified point in the cloud, the calculations presented earlier were repeated using only a single trajectory from cloud base to each insertion point. These trajectories still passed through the reference points in the cloud, but no mixing of different trajectories occurred there. In this test calculation, entrainment and mixing still affected the droplet size distribution as required to match cloud conditions along the selected droplet trajectory, but there was no broadening caused by mixing together of droplets following different trajectories. The result is shown in Fig. 17. There was considerable variability among the single trajectories that could be selected for this example, but it does show the typical result that a single trajectory leads to a much narrower droplet size distribution than the ensemble-average result and leads to fewer total embryos larger than either 40 or 50 µm diameter. Averaged over all insertion points, the single trajectories produced 0.126 cm^{-3} drops larger than 40 µm in diameter, and 0.0075 cm^{-3} larger than 50 µm in diameter, vs. 0.330 and 0.0135 cm^{-3} respectively for the ensemble-averaged cases that are the standard runs. In terms of total rainfall produced, the single-trajectory calculations produced about half as large a rainrate and total rainfall as the ensemble-average runs. This illustrates that, even along single trajectories with entrainment, there is sufficient production of embryos to account for significant rainfall, but rainfall production is also increased when mixing together of such trajectories broadens the droplet size distribution. The high contribution of single-trajectory runs to total rainfall and rainrate is consistent with the importance of giant nuclei, as discussed in the preceding section, because these giant nuclei are present in the single-trajectory calculations as well as in the ensemble-average calculations. Compared to the standard case, the reduction in rainfall when giant nuclei are excluded (1.9 mm h^{-1} to 0.7 mm h^{-1}, or 1.2 mm h^{-1}) is similar to the rainrate when only single trajectories are considered (1.1 mm h^{-1}). This supports the argument that the additional rainfall produced by coalescence in the modal peak of the

ACPD
11, 10557–10613, 2011

droplet size distribution arises (in this particular cloud) because of broadening of that main peak via the mechanism that is the central premise of this paper.

7.4 Variability arising near cloud base

The trajectories reaching a given location in the cloud originate from various locations at cloud base where updrafts vary, so this variability will contribute to broadening of the droplet size distribution. (cf., e.g., the arguments in Cooper (1989).) To estimate the importance of this contribution, calculations were repeated for which entrainment along the trajectories was suppressed. These trajectories duplicated the actual ascent times of entraining parcels, in order to include realistic times for broadening by coalescence. The mean droplet size of a representative set of 500 trajectories leading to a single point at the reference level was 30.29 µm and the standard deviation was 0.84 µm, while for the same trajectories the standard calculation with entrainment produced approximately the same mean size but gave a standard deviation of 4.33 µm. True adiabatic ascent produced a standard deviation of about 0.30 µm, so variability at cloud base does make a small contribution to the width of the droplet size distribution, but the dominant effect arises from variability in entrainment and mixing as discussed in Sect. 7.3.

7.5 Other sensitivities

Each of the preceding factors that influence the initiation of coalescence, and many others including the effects of turbulence, history of the liquid water content in the cloud, aerosol concentration, suppression of diffusional growth by surfactants, use of different collision efficiencies, and different assumptions regarding the nature of the mixing can be explored more fully using the framework developed in this paper. However, to keep the focus on the central premise of this study, those sensitivities will not be presented here.

ACPD
11, 10557–10613, 2011

8 Summary and conclusions

- Droplets that reach a specified location in a cumulus cloud follow varied trajectories to that location, and as a result can experience different effects of entrainment. The result is broadening of the droplet size distribution and the formation of embryos larger than 40 µm in diameter in much larger concentrations than without such broadening. This study has shown that, when this process is considered, the number of drizzle-size embryos is increased substantially in comparison to trajectories that do not consider such broadening by mixing.

- In the cloud studied, a small amount of rain formed via collision-coalescence in less than 20 min. While the rain is sufficient to account for approximately a 30 dBZ radar echo, the amount of such rain is still quite small and lower than typical for the clouds observed on the day that was the basis for this study. Nevertheless, the ability of the models to produce rain amounts in the range of observations is evidence that the processes being modelled are able to produce rainfall in the time available in a single small cumulus cell.

- The process emphasized in this study, the formation of drizzle via collisions among droplets in the main peak of the droplet size distribution, complements or competes with the growth of precipitation on giant nuclei. Both were important in the cloud studied, and neither is yet represented definitively, so their relative importance remains a subject of further study. Nevertheless, the mechanism developed as the central premise of this study is a significant contributor to the estimated rainfall from this cloud and so is an important candidate mechanism that may influence the formation of rain by warm-rain processes.

- Further enhancement of the process illustrated here is expected once other effects that enhance coalescence, especially the effects of turbulence on collisions among droplets, are included.

ACPD
11, 10557–10613, 2011

– While it appears that the process developed in this paper may not be the only, and perhaps in some cases not even the dominant, process involved in warm-rain formation, it is clearly important and should be considered as a candidate explanation in attempts to account for the formation of rain in warm clouds.

Appendix A

Changes to the microphysical model

A1 Treatment of inhomogeneous evaporation

Equation (3) from (LCB05) provides an estimate of the integral time scale of the subgrid-scale turbulence, and Eq. (3) from Cooper (1989) provides a similar estimate of the evaporation time, so these times are now compared and inhomogeneous evaporation is suppressed for drop sizes larger than the size for which these times are equal. This process uses the turbulent kinetic energy from the dynamical model and the drop size in the Lagrangian microphysical model to make the comparison, but as implemented the cut-off is sharp while it would be more realistic to have a variable cut-off that takes into account the variability in the intensity of turbulence at small scales. Including this transition avoids unrealistic evaporation of, for example, growing drizzle-size drops that are important embryos for the formation of rain.

An error was found and corrected in the representation of inhomogeneous evaporation as used in LCB05. The drop concentration for all bins was reduced as appropriate for mixing, then the liquid water content was calculated for the parcel, but the resulting water content was then erroneously reduced again for dilution; the proper order was to reverse the steps in the loop over drop sizes by calculating the liquid water content first and then reducing the drop concentrations for dilution upon entrainment. This led to an overestimate of the effect of inhomogeneous evaporation, which has now been corrected. (The previous paper used an adjustable parameter to scale the results between

Discussion Paper | Discussion Paper | Discussion Paper | Discussion Paper |

ACPD

11, 10557–10613, 2011

Initiation of coalescence in a cumulus cloud

W. A. Cooper et al.

fully homogeneous and fully inhomogeneous evaporation, so this error is equivalent to having more inhomogeneous evaporation than characterized by that adjustable parameter, by typically about a factor of 2.) This error does not change the conclusions of that paper.

The following provides the detailed manner in which this scheme is implemented:

1. Find the mixing fraction F of environmental air, with equivalent wet-bulb potential temperature Θ_q^{E}, in a unit of mixed air needed so that Θ_q^{P} of the resulting air parcel will match that of the cloud model, Θ_q^{C}:

$$F = \frac{\left(\Theta_q^{\mathrm{P}} - \Theta_q^{\mathrm{C}}\right)}{\left(\Theta_q^{\mathrm{P}} - \Theta_q^{\mathrm{E}}\right)} \tag{A1}$$

   To make the transition gradual, if $F > 0.1$, force $F = 0.1$ to provide a slower relaxation to the cloud-model values at each time step.

2. Adjust the parcel properties:

   – Adjust Θ_q of the parcel: $\Theta_q^{\mathrm{P}} \leftarrow \Theta_q^{\mathrm{P}}(1-F) + F\Theta_q^{\mathrm{E}}$. For F as in (A1), this sets the air-parcel equivalent wet-bulb potential temperature to the cloud-model value; otherwise, this moves the parcel value toward the cloud-model value.

   – Adjust parcel humidity variables [mixing ratio r and total-water mixing ratio r_t] in the same proportions. This results in a new supersaturation, after the new temperature is calculated, and the condensation/evaporation process will then continue as a natural part of ensuing calculations.

   – Dilute the [unactivated] entrained-CCN size distribution in the parcel by the factor $(1-F)$, then add $F n_{\mathrm{CCN}}^{\mathrm{E}}$where $n_{\mathrm{CCN}}^{\mathrm{E}}$ is the size distribution of CCN in the near-cloud environment.

3. Branch on evaporation type:

ACPD
11, 10557–10613, 2011

Discussion Paper | Discussion Paper | Discussion Paper | Discussion Paper |
Title Page
Abstract Introduction
Conclusions References
Tables Figures
◀◀ ▶▶
◀ ▶
Back Close
Full Screen / Esc
Printer-friendly Version
Interactive Discussion

- homogeneous evaporation: dilute the drop concentration, including any formed on entrained-CCN, by $(1-F)$;
- inhomogeneous evaporation, fraction f_{IH} $(0 < f_{\mathrm{IH}} <= 1)$:

i Find the portion of entrained air (F') that must mix with a portion $(1-F')$ of air from the cloud parcel to produce a just-saturated mixture. The portion F' is different from F; indeed, the wet-equivalent potential temperature of this initial saturated mixture, Θ_q^*, will generally differ from the final mixture, and the portion of the cloud drops not evaporated may remain in a supersaturated or subsaturated environment:

$$\Theta_q^* = (1-F')\Theta_q^{\mathrm{P}} + F'\Theta_q^{\mathrm{E}} \tag{A2}$$

$$r_t^* = (1-F')r_t^{\mathrm{P}} + F' r_t^{\mathrm{E}} \tag{A3}$$

If the result is to be just saturated, then the total water mixing ratio must satisfy

$$r_t^* = \frac{\varepsilon e_{\mathrm{s}}(T^*)}{p - e_{\mathrm{s}}(T^*)} \tag{A4}$$

where $e_{\mathrm{s}}(T^*)$ is the saturation vapour pressure at temperature T^*. The temperature of the intermediate just-saturated parcel, T^*, is then adjusted iteratively to satisfy the constraints (A2), (A3), and (A4).

ii Determine the fraction of drops, β, that must be evaporated completely to produce the saturated final mixture. This is related to the fraction of entrained air according to:

$$\beta = F\frac{1-F'}{F'(1-F)}. \tag{A5}$$

The value of β is then multiplied by f_{IH} to cause only that fraction of the water required to saturate the mixture to evaporate inhomogeneously. This makes

ACPD
11, 10557–10613, 2011

it possible to vary the nature of the evaporation from pure homogeneous to pure inhomogeneous by varying the variable f_{IH}.

iii Remove the fraction $f_{\mathrm{IH}}\beta$ of cloud drops from the size distribution and add this amount of water, evaporated, to the vapour pressure of the resulting mixture. However, limit the evaporation of large drops, as described above.

iv Dilute the resulting drop concentration as required by the addition of environmental air. In terms of the preceding variables, this requires that the drop concentration be multiplied by $(1-F)(1-f_{\mathrm{IH}}\beta)$ for all drops for which inhomogeneous evaporation is indicated, and by $(1-F)$ for all large drops for which homogeneous evaporation should apply.

v Adjust the number of unactivated CCN to include the remnants from the evaporated drops.

A2 Parcel trajectories

Another source of some criticism and discussion of LCB05 was the manner in which trajectories were treated in the Lagrangian microphysical model when the wet-equivalent potential temperature (Θ_q) increased along the trajectory. This occurs, for example, when the random-motion trajectories enter regions that in the cloud model are characterized by increasing temperature or humidity. Figure 5 shows some such trajectories. In the sense of turbulent mixing, this is a possible trajectory because an individual droplet can experience such a change in environment, but it is questionable how realistically this is represented in the random trajectories traced through the cloud model because only bulk characteristics of the turbulent motions are known at the grid scale of the model. To address this, three options were tested: (i) force a constant value of Θ_q when the model requires Θ_q to increase; (ii) impose a floor, so that a parcel never drops below the final Θ_q of the trajectory, avoiding unrealistically low values resulting when low values were encountered followed by subsequent increases to the final point; (iii) allow entrainment in a negative sense, that is, remove environmental air

ACPD
11, 10557–10613, 2011

from the parcel to increase its value of Θ_q to match that of the cloud model. By comparing results with these assumptions, it is possible to judge the uncertainty introduced by weakness in the representation of such processes.

The results presented in this paper are based on (iii). Other choices led to different droplet size distributions but did not change the basic conclusions of this paper. To illustrate the sensitivity to this choice, calculations to a specified reference point were made using each of these assumptions. The standard results quoted in this paper were that, for this point, 1.041 cm^{-3} embryos larger than 40 µm and 0.0300 cm^{-3} larger than 50 µm in diameter developed by the insertion point. In contrast, for options (i) and (ii), the corresponding results were 0.544 and 0.787 cm^{-3} embryos larger than 40 µm and 0.0157 and 0.0185 cm^{-3} larger than 50 µm. Either of these choices decreased the production of drizzle relative to the choice made in the present study, by amounts of about 50% or 25%, respectively. Choice (i) seems unrealistic because it tends to force the final parcel to be too dilute relative to the cloud model. However, (ii) and (iii) should provide limits to the true effects, so this comparison and other similar ones suggest that the uncertainty associated with this choice is on the order of 25% or less.

A3 The CCN size distribution

Some questions have arisen in connection with the definition of the cumulative CCN supersaturation distribution as used in Cooper et al. (1997), so that definition is documented in more detail here. Changes are also imposed because it appeared that the distribution as used there included an unreasonable contribution at very large sizes (greater than 25 µm diameter), so the representation was changed to make it possible to eliminate these very large CCN while still providing a complete size distribution of the particles assumed to be CCN. As in the preceding paper, we assume the CCN to be soluble and composed of ammonium sulphate, but the results are not sensitive to the specific chemical composition as long as the substance is assumed completely and readily soluble. Possible effects of mixed composition, surfactants that might affect

Discussion Paper | Discussion Paper | Discussion Paper | Discussion Paper |

ACPD

11, 10557–10613, 2011

the condensation coefficient, or other effects of organic aerosols are not included in the calculations presented here.

We follow standard references (e.g., Pruppacher and Klett, 1997) to obtain the critical supersaturation for activation, S_c, in terms of the dry particle size:

$$\ln S_c = \frac{C^*}{r_s^{3/2}} \tag{A6}$$

where

$$C^* = \frac{2A^{3/2}}{(27B)^{1/2}(4\pi\rho_s/3)^{1/2}}$$

$$A = 2\sigma M_w/(\rho_s RT)$$

$$B = 3iM_w/(4\pi\rho_s M_s)$$

and S_c is the critical supersaturation for activation of the CCN (at supersaturation SS such that $S_c = 1 + (\mathrm{SS}/100\%)$), ρ_s is the density of the soluble particle, σ the surface tension of the solution droplet, M_w the molecular weight of water, R the universal gas constant, T the temperature of the solution droplet, and i the van't Hoff factor for the salt in solution.

If the differential distribution functions associated with the cumulative distribution functions $n(\mathrm{SS})$ and $N(r_s)$ are, respectively, $f(\mathrm{SS})$ and $F(r_s)$, and if SS/(100%) is small compared to unity, then

$$\frac{\mathrm{SS}}{100\%} \approx C^* r_s^{-3/2}$$

gives the relationship between critical supersaturation SS and the size of the particle r_s. Then, from $F(r)dr = -f(\mathrm{SS})d\mathrm{SS}$,

$$F(r_s) = -Ck(100\mathrm{SS})^{k-1}\frac{d\mathrm{SS}}{dr_s}$$

Discussion Paper | Discussion Paper | Discussion Paper | Discussion Paper |
ACPD
11, 10557–10613, 2011

Initiation of coalescence in a cumulus cloud

W. A. Cooper et al.

or

$$F(r) = C' r^{\alpha} \tag{A7}$$

where $C' = 1.5Ck(100C^*)^k$ and $\alpha = -\frac{3}{2}(k-1) - \frac{5}{2} = -\frac{3}{2}k - 1$. Equation (A7) then specifies the size distribution in terms of the parameters of the CCN spectrum.

The total mass of the size distribution is

$$M = \int F(r_s)\frac{4}{3}\pi r_s^3 \rho_s dr_s \sim r_s^{4+\alpha}$$

so, to avoid having the large-size part of the distribution contribute an infinite mass, it is necessary that α be smaller than -4. This requires $k > 2$, a condition seldom met by measured CCN spectra. For this reason, it is necessary to combine the CCN spectrum with one at large sizes that has a steeper decreasing slope with size. One candidate is the Junge cumulative size distribution $N_J(r_s)$, suggested as valid for sizes larger than radii of $r_1 = 0.1$ µm and specified as

$$\frac{dN_J(r_s)}{d\log_{10}(r_s)} = \frac{A_J}{r_s^3} \tag{A8}$$

where $A_J = 10^{-13}$. In this form, A_J is dimensionless. The differential size distribution $F_J(r_s) = dN_J(r_s)/dr_s$ is then

$$F_J(r_s) = \frac{A_J}{\ln(10) r_s^4}. \tag{A9}$$

A property of the Junge size distribution is that all logarithmic intervals contribute equally to the mass, so again some truncation or modification is needed at large size. If the upper limit to this size distribution is taken to be r_2, the concentration between radii r_1 and r_2 becomes

$$\int F_J(r_s) dr_s = \frac{A_J}{3\ln(10)}\left(\frac{1}{r_1^3} - \frac{1}{r_2^3}\right). \tag{A10}$$

Discussion Paper | Discussion Paper | Discussion Paper | Discussion Paper |

ACPD

11, 10557–10613, 2011

Initiation of coalescence in a cumulus cloud

W. A. Cooper et al.

At the largest sizes, the evidence presented by Alofs and Liu (1981) argues for a steeper descent, for which $dN_A(r_s)/d\log_{10}r_s = A_A r_s^{-\beta}$ with $\beta = 4$. This provides the desired result of having a full size distribution function with finite mass at the largest sizes. A transition to this might reasonably be made at a radius of r_2 =1 µm.

The following is the procedure used to match these distributions at the transition sizes:

a First consider the transition from the Junge region to the largest-size region, assumed to occur at r_J. If $N_A(r_s) \sim r_s^{1-\beta}$, $dN_A/d\log_{10}r_s = A_A r_s^{-\beta}$, so to match to the Junge distribution at $r_s = r_J$ it is necessary that

$$\frac{dN_J}{d\log r_s} = \frac{dN_A}{d\log r_s}$$

or

$$\frac{A_J}{r_J^3} = \frac{A_A}{r_j^{\beta}}$$

so

$$A_A = A_J r_j^{\beta-3} \tag{A11}$$

The cumulative number of CCN with sizes larger than r_s in the largest-size region, for $r_s > r_A$, is then

$$N_A(r_s) = A_A \frac{\beta}{\ln 10} r_s^{-\beta} \tag{A12}$$

– For the transition from the small-size region specified as $C(\mathrm{SS}/100)^k$ to the Junge distribution, the size at which the transition occurs is specified as $r_t = 0.1$ µm radius. Then, with the slope specified for the Junge distribution, the concentration

ACPD
11, 10557–10613, 2011

is adjusted to match that from the small-CCN distribution at that size. This gives a continuous cumulative size distribution function, although there is a discontinuity in the differential size distribution. This has not produced an apparent gap in the initialized size distribution.

The Junge integral then gives a cumulative number from r_t upward of $A_J/(3\ln(10)r_t^3)$. The corresponding supersaturation is $SS/100 = C^* r_t^{-3/2}$ so matching the cumulative distribution functions gives:

$$CC^{*^k} r_t^{-3k/2} = \frac{A_J}{3\ln(10)r_t^3}$$

or

$$A_J = 3\ln(10)CC^{*^k} r_t^{3-3k/2} \tag{A13}$$

The size distribution is then specified by the parameters C and k of the small-size distribution function, the lower and upper limits (r_1, r_2) for which to use the Junge distribution, and the power law dependence β assumed for the largest sizes. In addition, a cut-off size is imposed to avoid some of the largest ultra-giant aerosols. For the calculations presented in this paper, the choices were $C = 365\,\mathrm{cm}^{-3}$, $k = 0.23$, Junge lower and upper limits of 0.2 and 2 µm diameter, and a power-law dependence as $\beta = 4$ as specified above. The ultra-giant aerosol population was also truncated at a diameter of 50 µm, but tests with this truncation extended to 1000 µm showed negligible effect on the rainfall. The corresponding cumulative size distribution for CCN composed of ammonium sulphate is shown in Fig. A1. This figure is reasonably consistent with the summary figure of previous observations presented by Jensen and Lee (2008) (their Fig. 1), except at the highest wind speeds where it would underestimate the giant-nucleus concentration.

For entrained CCN, there is little basis for a choice. The assumption was made that entrained CCN are similar in size distribution but have a concentration half as large as the CCN entering through cloud base.

ACPD
11, 10557–10613, 2011

Acknowledgements. The National Center for Atmospheric Research is sponsored by the National Science Foundation. Support for the second author was provided by the NSF grant ATM-0342421. Most of the numerical modelling for this study was conducted on the supercomputers of the Computational and Information Systems Laboratory at the National Center for Atmospheric Research (NCAR). Photorealistic renderings of the cloud simulation and associated trajectories were made with software developed under NSF grant IIS-0513464.

References

Alofs, D. J. and Liu, T. H.: Atmospheric measurements of CCN in the supersaturation range 0.013–0.681-percent, J. Atmos. Sci., 38, 2772–2778, 1981. 10590

Andrejczuk, M., Grabowski, W. W., Malinowski, S. P., and Smolarkiewicz, P. K.: Numerical simulation of cloud-clear air interfacial mixing: Effects on cloud microphysics, J. Atmos. Sci., 63, 3204–3225, 2006. 10568, 10569

Baker, M. B. and Latham, J.: Evolution of droplet spectra and the rate of production of embryonic raindrops in small Cumulus clouds, J. Atmos. Sci., 36, 1612–1615, 1979. 10565, 10568

Baker, M. B., Corbin, R. G., and Latham, J.: The influence of entrainment on the evolution of cloud droplet spectra .1. A model of inhomogeneous mixing, Q. J. Roy. Meteor. Soc., 106, 581–598, 1980. 10559

Bartlett, J. T. and Jonas, P. R.: Dispersion of sizes of droplets growing by condensation in turbulent clouds, Q. J. Roy. Meteor. Soc, 98, 150, 150–164, 1972. 10561

Beard, K. V.: Terminal velocity and shape of cloud and precipitation drops aloft, J. Atmos. Sci., 33, 851–864, 1976. 10573

Beard, K. V. and Ochs, H. T.: Warm-rain initiation – An overview of microphysical mechanisms, J. Appl. Meteorol., 32, 608–625, 1993. 10558, 10575

Blyth, A. M., Lasher-Trapp, S. G., Cooper, W. A., Knight, C., and Latham, J.: The role of giant and ultragiant nuclei in the formation of early radar echoes in warm cumulus clouds, J. Atmos. Sci., 60, 2557–2572, 2003. 10558

Carpenter, R. L., Droegemeier, K. K., and Blyth, A. M.: Entrainment and detrainment in numerically simulated cumulus congestus clouds. Part I: General results, J. Atmos. Sci., 55, 3417–3432, 1998. 10563

Caylor, I. J. and Illingworth, A. J.: Radar observations and modeling of warm rain initiation, Q. J. Roy. Meteor. Soc., 113, 1171–1191, 1987. 10578
Cooper, W. A.: Effects of variable droplet growth histories on droplet size distributions .1. Theory, J. Atmos. Sci., 46, 1301–1311, 1989. 10559, 10560, 10562, 10581, 10583
Cooper, W. A., Bruintjes, R. T., and Mather, G. K.: Calculations pertaining to hygroscopic seeding with flares, J. Appl. Meteorol., 36, 1449–1469, 1997. 10564, 10587
Fankhauser, J. C.: Estimates of thunderstorm precipitation efficiency from field-measurements in CCOPE, Mon. Weather Rev., 116, 663–684, 1988. 10576
Ferrier, B. S., Simpson, J., and Tao, W. K.: Factors responsible for precipitation efficiencies in midlatitude and tropical squall simulations, Mon. Weather Rev., 124, 2100–2125, 1996. 10576
Goke, S., Ochs, H. T., and Rauber, R. M.: Radar analysis of precipitation initiation in maritime versus continental clouds near the Florida coast: Inferences concerning the role of CCN and giant nuclei, J. Atmos. Sci., 64, 3695–3707, doi:10.1175/JAS3961.1, 2007. 10558
Illingworth, A. J.: The formation of rain in convective clouds, Nature, 336, 754–756, 1988. 10578
Illingworth, A. J. and Caylor, I. J.: Radar observations and modeling of warm rain initiation, Annalen der Meteorologie, 25, 49–51, 1988. 10578
Jensen, J. B. and Lee, S.: Giant Sea-Salt Aerosols and Warm Rain Formation in Marine Stratocumulus, J. Atmos. Sci., 65, 3678–3694, doi:10.1175/2008JAS2617.1, 2008. 10591
Jensen, J. B., Austin, P. H., Baker, M. B., and Blyth, A. M.: Turbulent mixing, spectral evolution and dynamics in a warm Cumulus cloud, J. Atmos. Sci., 42, 173–192, 1985. 10569
Johnson, D. B.: The role of giant and ultra-giant aerosol-particles in warm rain initiation, J. Atmos. Sci., 39, 448–460, 1982. 10559, 10578
Jonas, P. R. and Mason, B. J.: Entrainment and the droplet spectrum in Cumulus clouds, Q. J. Roy. Meteor. Soc., 108, 857–869, 1982. 10559
Jonas, P. R. and Mason, B. J.: Entrainment and the droplet spectrum in Cumulus clouds – Reply, Q. J. Roy. Meteor. Soc., 109, 899–900, 1983. 10559
Knight, C. A., Vivekanandan, J., and Lasher-Trapp, S. G.: First radar echoes and the early Z(DR) history of Florida cumulus, J. Atmos. Sci., 59, 1454–1472, 2002. 10578
Laird, N. F., Ochs, H. T., Rauber, R. M., and Miller, L. J.: Initial precipitation formation in warm Florida cumulus, J. Atmos. Sci., 57, 3740–3751, 2000. 10558
Lasher-Trapp, S. G., Knight, C. A., and Straka, J. M.: Early radar echoes from ultragiant aerosol

ACPD
11, 10557–10613, 2011

in a cumulus congestus: Modeling and observations, J. Atmos. Sci., 58, 3545–3562, 2001. 10559, 10563, 10565, 10572
Lasher-Trapp, S. G., Cooper, W. A., and Blyth, A. M.: Measurements of ultragiant aerosol particles in the atmosphere from the small cumulus microphysics study, J. Atmos. Ocean. Technol., 19, 402–408, 2002. 10578
Lasher-Trapp, S. G., Cooper, W. A., and Blyth, A. M.: Broadening of droplet size distributions from entrainment and mixing in a cumulus cloud, Q. J. Roy. Meteor. Soc., 131, 195–220, doi:10.1256/qj.03.199, 2005. 10560, 10562
Lehmann, K., Siebert, H., and Shaw, R. A.: Homogeneous and inhomogeneous mixing in Cumulus clouds: Dependence on local turbulence structure, J. Atmos. Sci., 66, 3641–3659, doi:10.1175/2009JAS3012.1, 2009. 10569
MacPherson, J. and Isaac, G.: Turbulent characteristics of some Canadian Cumulus clouds, J. Appl. Meteorol., 16, 81–90, 1977. 10560
Ochs, H. T.: Moment-conserving techniques for warm cloud microphysical computations .2. Model testing and results, J. Atmos. Sci., 35, 1959–1973, 1978. 10559
Pinsky, M., Khain, A., and Shapiro, M.: Collisions of small drops in a turbulent flow. Part I: Collision efficiency. problem formulation and preliminary results, J. Atmos. Sci., 56, 2585–2600, 1999a. 10559
Pinsky, M. B., Khain, A. P., and Levin, Z.: The role of the inertia of cloud drops in the evolution of the spectra during drop growth by diffusion, Q. J. Roy. Meteor. Soc., 125, 553–581, 1999b. 10559
Pruppacher, H. R. and Klett, J. D.: Microphysics of Clouds and Precipitation, Kluwer Academic, Dordrecht, 2nd edn., 1997. 10588
Saffman, P. G. and Turner, J. S.: On the collision of drops in turbulent clouds, J. Fluid Mech., 1, 16–30, doi:10.1017/S0022112056000020, 1956. 10559
Shaw, R. A., Reade, W. C., Collins, L. R., and Verlinde, J.: Preferential concentration of cloud droplets by turbulence: Effects on the early evolution of cumulus cloud droplet spectra, J. Atmos. Sci., 55, 1965–1976, 1998. 10559
Small, J. D. and Chuang, P. Y.: New observations of precipitation initiation in warm cumulus clouds, J. Atmos. Sci., 65, 2972–2982, doi:10.1175/2008JAS2600.1, 2008. 10574, 10575
Srivastava, R. C.: Growth of cloud drops by condensation – A criticism of currently accepted theory and a new approach, J. Atmos. Sci., 46, 869–887, 1989. 10559
Straka, J. M. and Anderson, J. R.: Numerical simulations of microburst-producing storms –

some results from storms observed during COHMEX, J. Atmos. Sci., 50, 1329–1348, 1993. 10563

Telford, J. W. and Chai, S. K.: A new aspect of condensation theory, Pure Appl. Geophys., 118, 720–742, 1980. 10559

Wang, L.-P., Ayala, O., Rosa, B., and Grabowski, W. W.: Turbulent collision efficiency of heavy particles relevant to cloud droplets, New J. Phys., 10, doi:10.1088/1367-2630/10/7/075013, 2008. 10559

Warner, J.: The microstructure of Cumulus cloud .1. General features of the droplet spectrum, J. Atmos. Sci., 26, 1049–1059, 1969. 10562

Woodcock, A. H.: Atmospheric salt particles and raindrops, J. Meteorol., 9, 200–212, doi:10.1175/1520-0469(1952)009¡0200:ASPAR¿2.0.CO;2, 1952. 10578

Woodcock, A. H.: Salt nuclei in marine air as a function of altitude and wind force, J. Meteorol., 10, 362–371, doi:10.1175/1520-0469(1953)010¡0366:SNIMAA¿2.0.CO;2, 1953. 10578

Woodcock, A. H.: Marine fog droplets and salt .1., J. Atmos. Sci., 35, 657–664, 1978. 10578

Woodcock, A. H., Duce, R. A., and Moyers, J. L.: Salt Particles and Raindrops in Hawaii, J. Atmos. Sci., 28, 1252–1257, doi:10.1175/1520-0469(1971)028¡1252:SPARIH¿2.0.CO;2, 1971. 10578

Yum, S. S. and Hudson, J. G.: Microphysical relationships in warm clouds, Atmos. Res., 57, 81–104, 2001. 10567

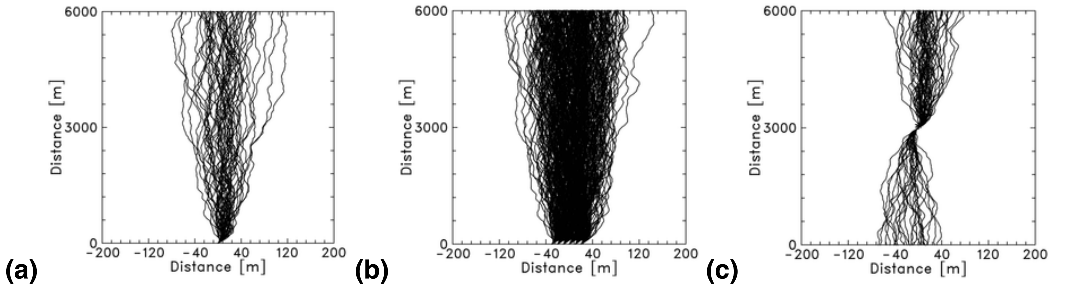

Fig. 1. **(a)** Random-simulation trajectories from a point source using conditions described in the text. **(b)** A similar simulation but with sources at seven locations spaced at 10-m increments across the cloud base. **(c)** Random trajectories that pass through a specified point in the cloud.

ACPD
11, 10557–10613, 2011

Initiation of coalescence in a cumulus cloud

W. A. Cooper et al.

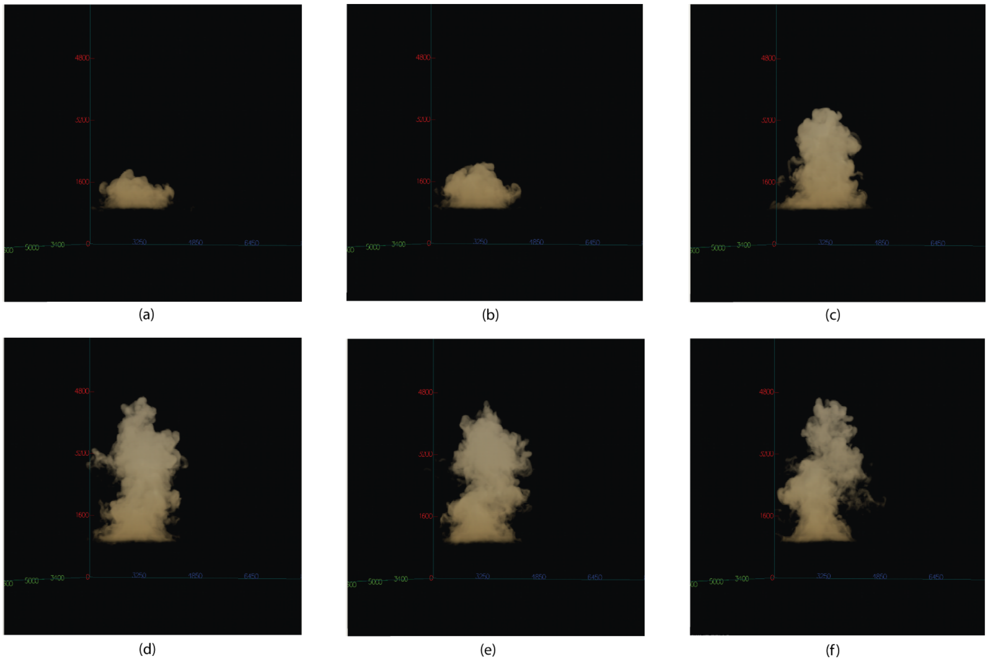

Fig. 2. Time series of photo-realistic renderings of a multi-thermal cloud simulation representative of that occurring on 10 August 1995 during the Small Cumulus Microphysics Study. Approximate simulation times are: **(a)** 2 min; **(b)** 4 min; **(c)** 10 min; **(d)** 16 min; **(e)** 18 min; and **(f)** 21.75 min after the first appearance of the cloud.

ACPD
11, 10557–10613, 2011

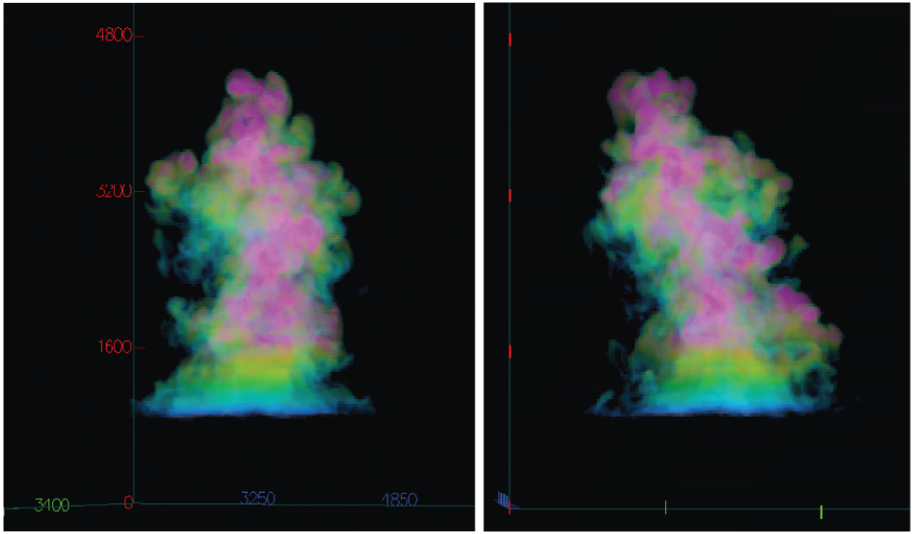

Fig. 3. Photo-realistic renderings (front view shown to left; side view shown to right) of the same simulated cloud as in Fig. 2, at 14 min after the start of the cloud, showing variability in the cloud water. Colour shading indicates ranges of cloud water mixing ratio: dark blue, 0–1 $g\,kg^{-1}$; turquoise, 1–2 $g\,kg^{-1}$; green, 2–3 $g\,kg^{-1}$; yellow, 3–4 $g\,kg^{-1}$; and pink, greater than 4 $g\,kg^{-1}$.

ACPD
11, 10557–10613, 2011

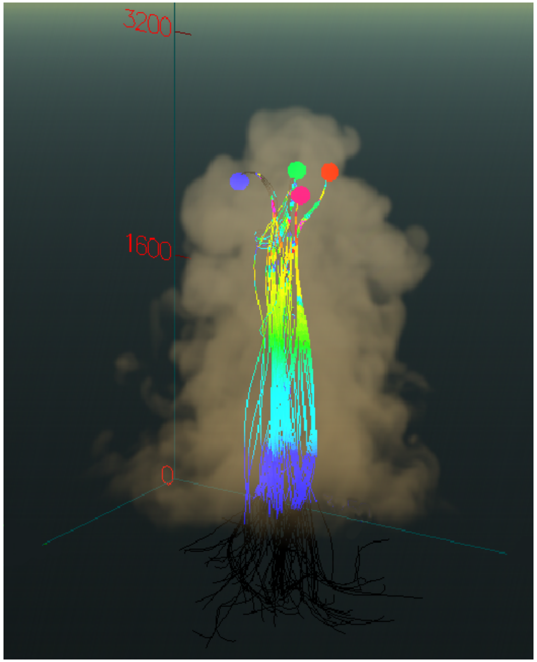

Fig. 4. Photo-realistic rendering of the simulated cloud at 10 min after the start of the cloud, overlaid with the entire history of a small subset of the droplet trajectories ascending to four of the reference points. The variability of the trajectories leading up to any given point on the grid contributes to the diversity in droplet sizes, shown later. Colours along the trajectories indicate the amount of cloud water at the trajectory location, ranging from dark blue (lowest cloud water) to magenta (highest cloud water content). The labels on the vertical axis are height in metres.

ACPD
11, 10557–10613, 2011

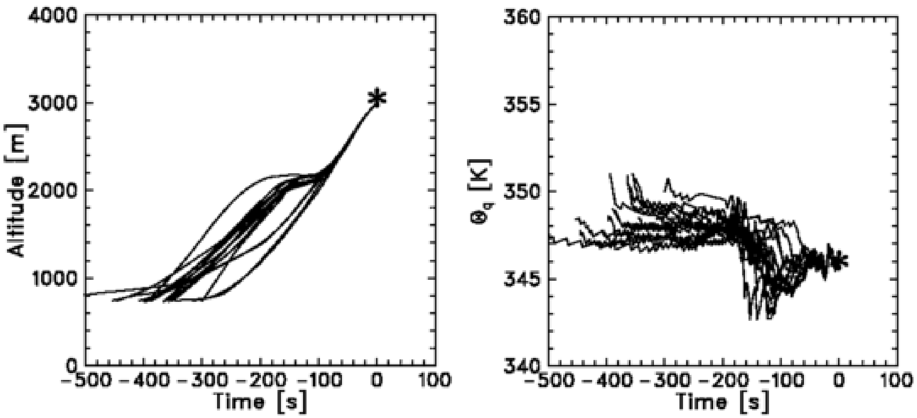

Fig. 5. Examples of individual trajectories that arrive at a reference point (denoted by the large asterisk).

Discussion Paper | Discussion Paper | Discussion Paper | Discussion Paper |

ACPD

11, 10557–10613, 2011

Initiation of coalescence in a cumulus cloud

W. A. Cooper et al.

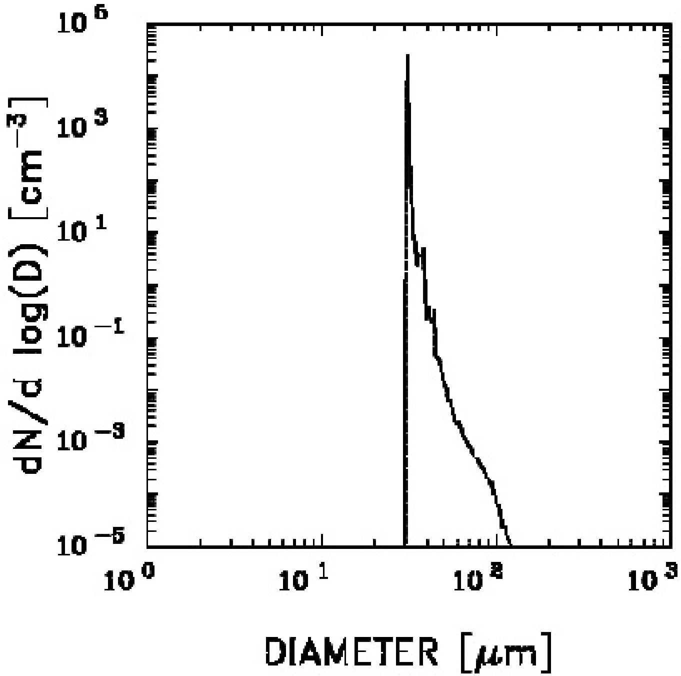

Fig. 6. The droplet size distribution calculated for adiabatic ascent from cloud base to 3 km MSL. This ascent of 2.3 km took 254 s, and the resulting droplet concentration was 272 cm^{-3}, the mean diameter was 31.2 μm with a standard deviation of 0.30 μm, the liquid water content was 4.31 $g\,m^{-3}$, and there were 0.016 cm^{-3} droplets larger than 40 μm in diameter.

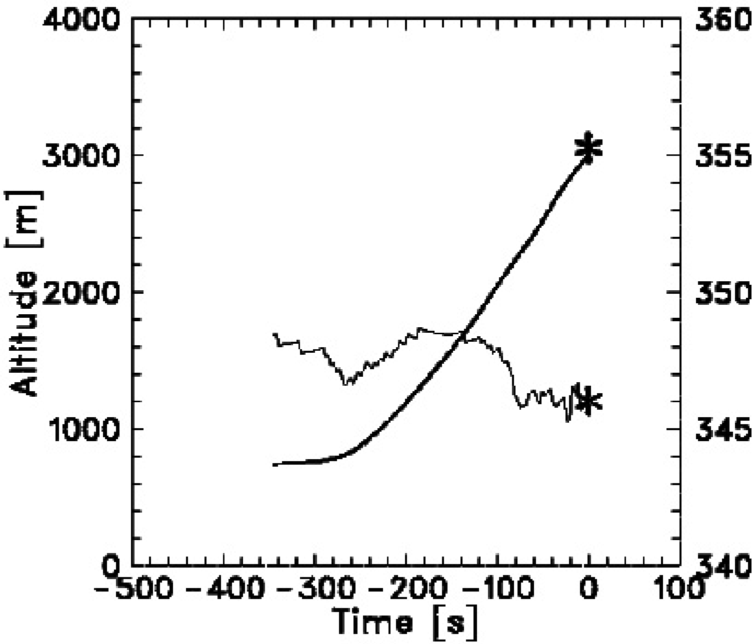

Fig. 7. A trajectory selected from the ensemble of randomly generated trajectories that reach the same point as used for Fig. 6. The thick line is the altitude relative to the left-side scale; the thin line is the wet-equivalent potential temperature θ_q relative to the right-side scale. This is a rapidly ascending example that still experiences significant mixing.

ACPD
11, 10557–10613, 2011

Initiation of coalescence in a cumulus cloud

W. A. Cooper et al.

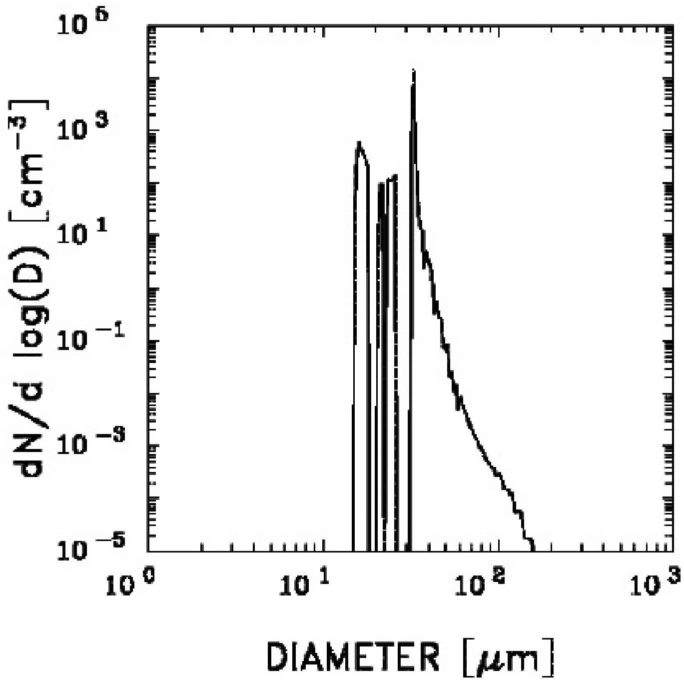

Fig. 8. Droplet size distribution calculated along a specific trajectory, selected from the randomly generated ensemble, that reaches the same point as represented in Fig. 6. The final droplet concentration was 218 cm^{-3}, the mean diameter was 30.5 µm with a standard deviation of 5.6 µm, and the concentration of drops larger than 40 µm in diameter was 0.082 cm^{-3}.

ACPD
11, 10557–10613, 2011

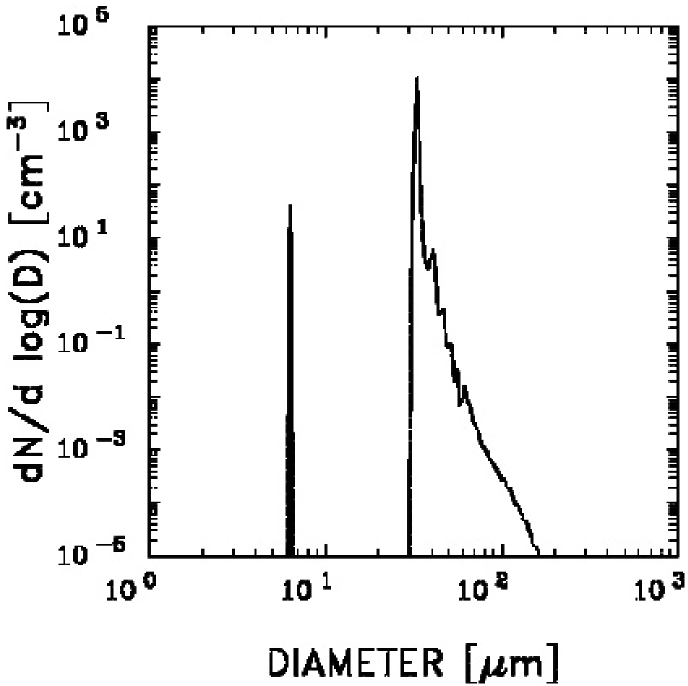

Fig. 9. Droplet size distribution for another trajectory with entrainment typical of the ensemble of trajectories reaching the reference point in the cloud. The final liquid water content was 3.44 g m^{-3}, the mean diameter was 33.4 μm with a standard deviation of 1.69 μm, and the concentration of drops larger than 40 μm in diameter was 0.148 cm^{-3}.

ACPD
11, 10557–10613, 2011

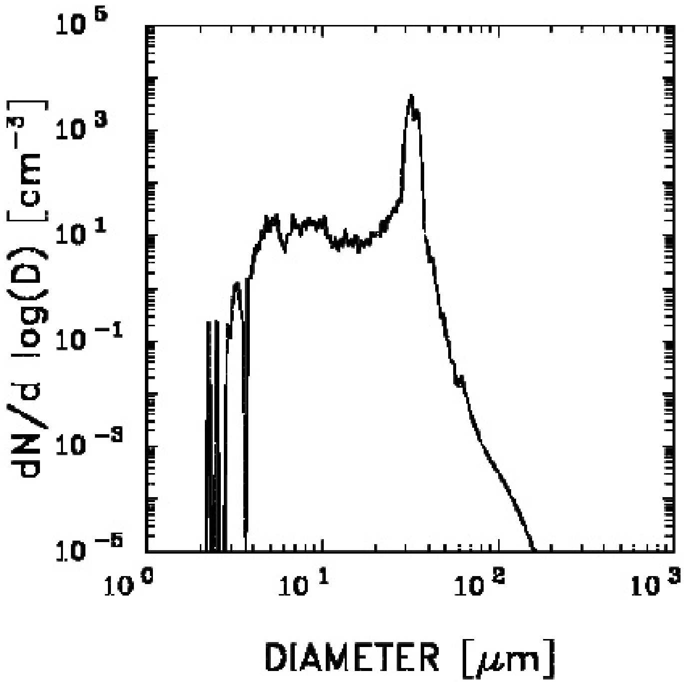

Fig. 10. Droplet size distribution obtained by averaging the randomly simulated trajectories that reach the reference point in the cloud described in the text. The final droplet concentration was 220 cm^{-3} liquid water content 3.37 $g\,m^{-3}$, mean diameter 29.4 μm with standard deviation of 7.0 μm, and the concentration of drops larger than 40 μm in diameter was 0.134 cm^{-3} with 0.007 cm^{-3} larger than 50 μm.

ACPD
11, 10557–10613, 2011

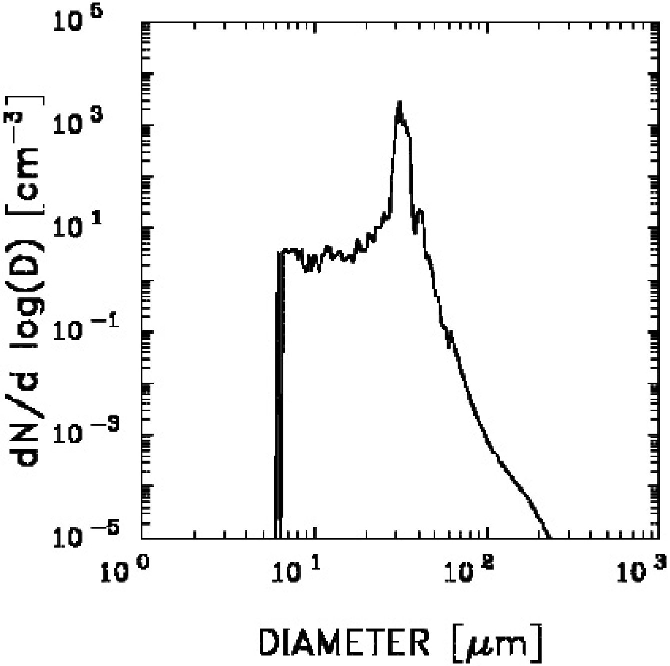

Fig. 11. The droplet size distribution corresponding to Fig. 10, after an additional 120 s of growth along a trajectory corresponding to the mean air motion in the cloud.

ACPD
11, 10557–10613, 2011

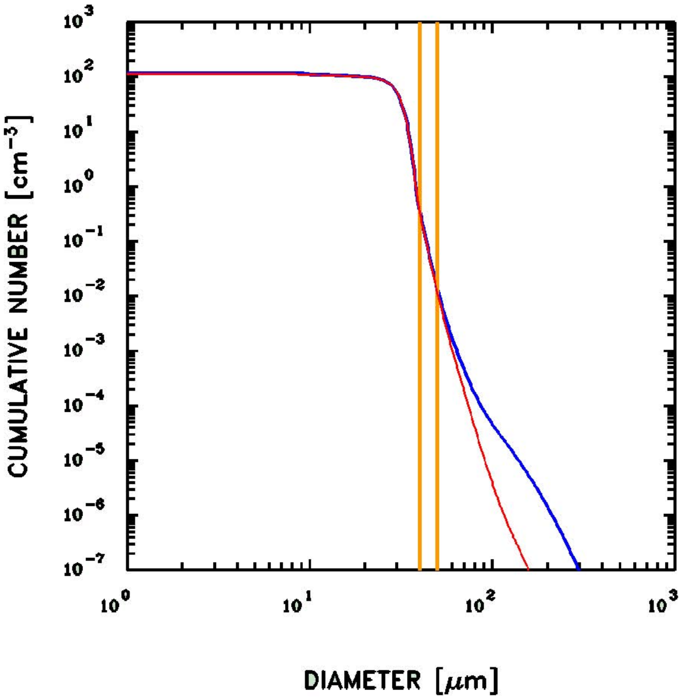

Fig. 12. Cumulative drop size distribution averaged over all 57 insertion points producing embryos in the microphysical model ("initial embryos"), and cumulative size distribution at the end of the continuous collection calculations ("final drizzle/raindrops"). The final size distribution includes all drops located anywhere in the cloud along their respective trajectories, as if returned to their initial colocated concentration at insertion time.

ACPD
11, 10557–10613, 2011

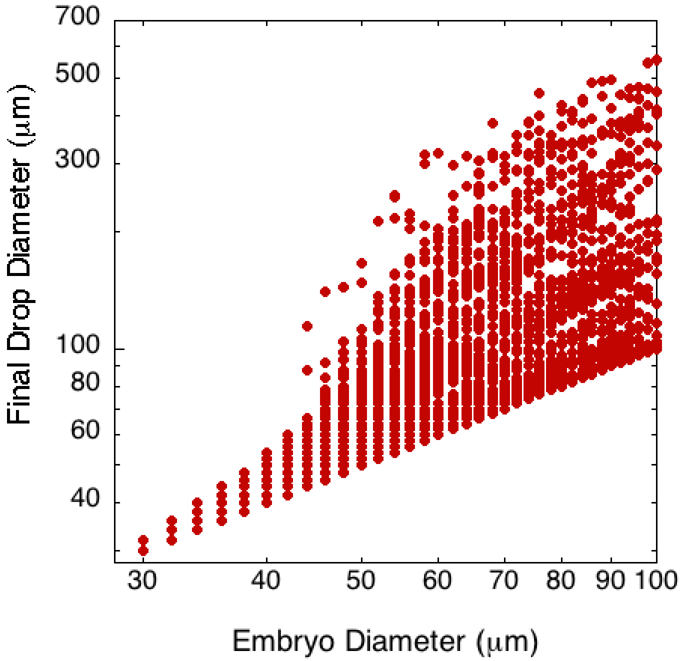

Fig. 13. Initial embryo size versus final drop size from the continuous collection calculations. Many of the points are obscured because they lie on top of one another.

ACPD
11, 10557–10613, 2011

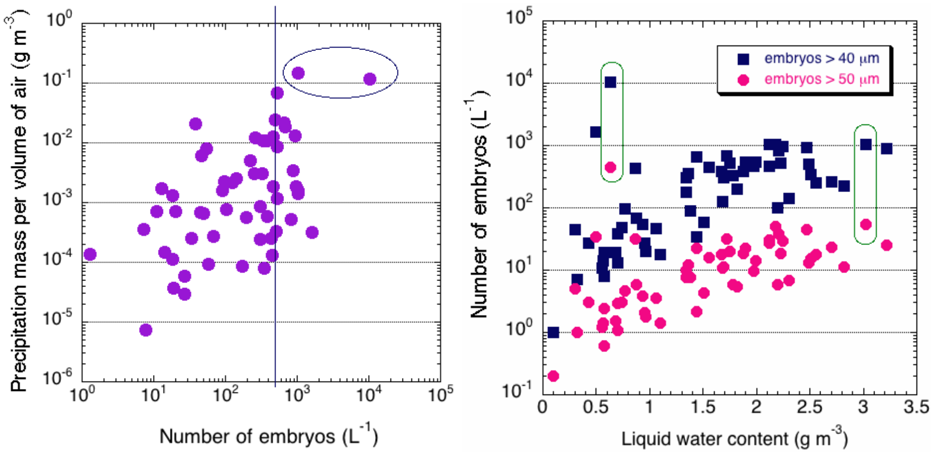

Fig. 14. For all insertion points in the cloud: (left) number of embryos exceeding 40 µm diameter produced at each point versus the precipitation mass (for drops exceeding 200 µm diameter) attributable to those embryos, and (right) the initial cloud water content at a given point versus the number of embryos exceeding either 40 or 50 µm in diameter. Points lying within ovals are discussed in the text, and the vertical line in the top figure separates points having in excess of 0.5 cm^{-3} or 500/litre embryos.

ACPD
11, 10557–10613, 2011

Initiation of coalescence in a cumulus cloud

W. A. Cooper et al.

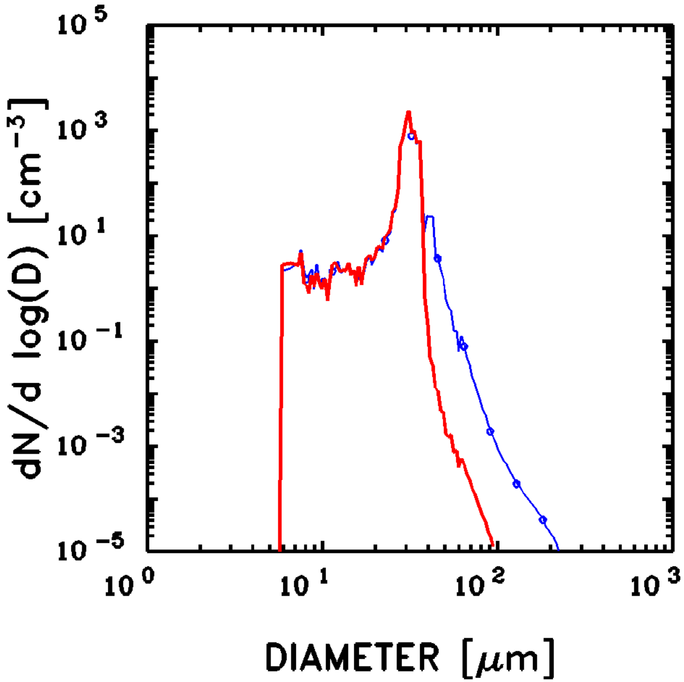

Fig. 15. Comparison of the drop size distribution obtained with coalescence suppressed (thick red line) to standard results with coalescence (thin blue line with dots), for trajectories reaching reference point 84 and then carried forward to the insertion point. These are the embryos available for continued growth to rain.

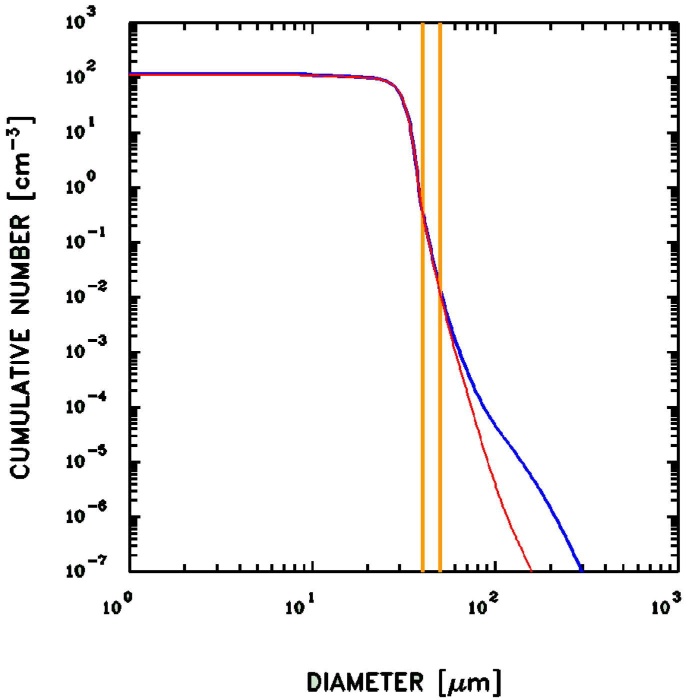

Fig. 16. Cumulative drop size distribution for the standard calculations (blue thick line) and for a test calculation (red thin line) for which all CCN with dry diameter exceeding 2 μm in diameter were eliminated from the input CCN size distribution. The orange lines denote 40 μm and 50 μm diameters, limits used in the text for measures of embryo production.

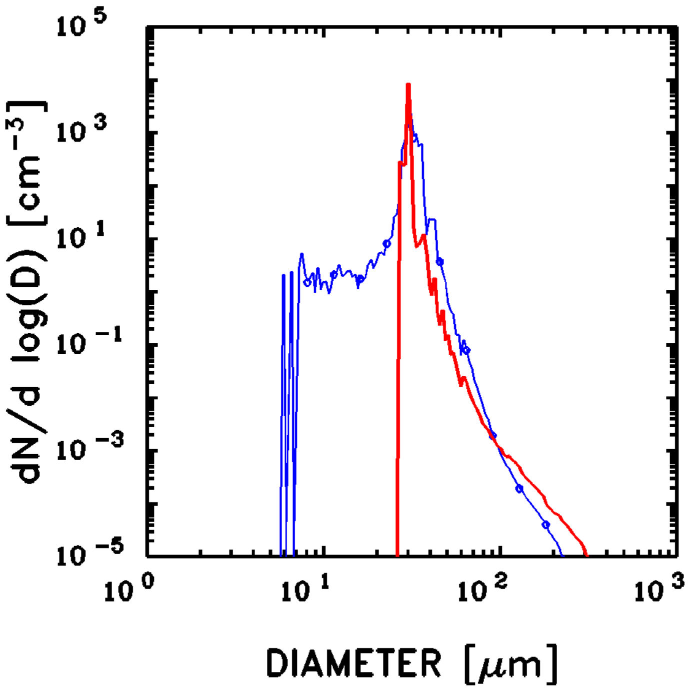

Fig. 17. The drop size distribution produced by a specific trajectory that passes through reference point 84 (thick red line), compared to the size distribution that results from averaging 500 trajectories all reaching that same point (thin blue line with dots). In each case, the trajectory was carried forward from the reference point 120 s to determine the size distribution inserted into the cloud-water fields to determine growth to rain. (While the drop size distribution for the single-trajectory case selected has more drops with diameters exceeding 100 μm than does the ensemble-average size distribution, that is an accident of the selection; other single-trajectory cases leading to this same point have lower concentrations at this threshold so that the average is as shown by the thin blue line.)

ACPD
11, 10557–10613, 2011

Initiation of coalescence in a cumulus cloud

W. A. Cooper et al.

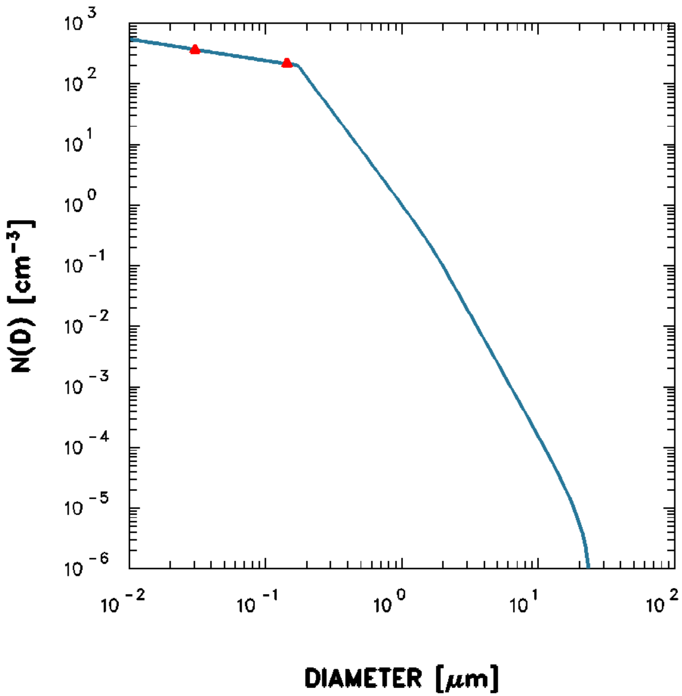

Fig. A1. Cumulative aerosol size distribution used in this study. The particles are assumed soluble (ammonium sulphate). The three regions are: (i) less than 0.2 µm diameter, power law in activation supersaturation characterized by $C = 365\,\text{cm}^{-3}$ and $k = 0.2$; (ii) 0.2 to 2 µm diameter, a Junge power law; and (iii) greater than 2 µm, size distribution decreases as diameter^{-4}. Two red dots denote the 0.1% and 1% critical supersaturation points. The size distribution is truncated to eliminate ultra-giant nuclei with diameters above 25 µm.

ACPD
11, 10557–10613, 2011

Initiation of coalescence in a cumulus cloud

W. A. Cooper et al.